THE JOURNAL OF PHYSICAL CHEMISTRY Letters

Letter

Cite This: J. Phys. Chem. Lett. 2019, 10, 5244−5249

pubs.acs.org/JPCL

Substitution Dependent Ultrafast Ultraviolet Energy Dissipation Mechanisms of Plant Sunscreens

Xi Zhao,[†,‡,⊥] Jian Luo,[†,⊥] Yan Liu,[†] Pramod Pandey,[†] Songqiu Yang,[†] Donghui Wei,[§] and Keli Han*[,†,∥]

[†]State Key Laboratory of Molecular Reaction Dynamics, Dalian Institute of Chemical Physics (DICP), Chinese Academy of Sciences, 457 Zhongshan Road, Dalian, Liaoning 116023, China

[‡]University of Chinese Academy of Sciences, Beijing 10049, China

[§]College of Chemistry and Molecular Engineering, Zhengzhou University, 100 Science Avenue, Zhengzhou, People's Republic of China

[∥]Institute of Molecular Sciences and Engineering, Shandong University, Qingdao 266237, P. R. China

Supporting Information

ABSTRACT: An ultraviolet energy dissipation mechanism plays a critical role in the photoprotection effect of sunscreens. In this work, we discovered substitution dependent UV energy dissipation mechanisms of model plant sunscreen methyl sinapate (MS). We found that the initially populated V($\pi\pi^*$) states of MS and *p*-OMeMS relax to the ground state nonradiatively along an ultrafast trans−cis photoisomerization in tens of picoseconds. However, for *p*-HMS, an internal conversion from V($\pi\pi^*$) to a relative dark V′($\pi\pi^*$) state occurs in less than 1 ps, leading to a branching of the excited-state relaxations. The V($\pi\pi^*$) state still relaxes nonradiatively as in the case of MS and *p*-OMeMS. In contrast, the V′($\pi\pi^*$) state decays to the ground state mainly by emitting photons, exhibiting a lifetime as long as 5 ns. It is the first time to definitely distinguish the dynamics between V($\pi\pi^*$) and V′($\pi\pi^*$) states in the study of sinapates and cinnamates. These results indicate the anticipation of the V′($\pi\pi^*$) state should be avoided when designing sunscreens.

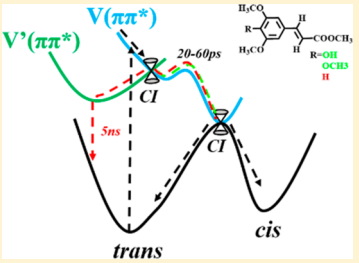

Excessive exposure to ultraviolet (UV) radiation would cause photoaging, photosensitivity, and DNA damage.[1−4] Various sunscreens, such as oxybenzone[5] and cinnamate-based molecules,[6−8] are designed to protect skin from damage by UV light. The efficiency of UV energy dissipation of sunscreens after absorbing UV radiation is an important factor for high performance sunscreens.[9−11] The more efficient the dissipation of UV energy to the electronic ground state (S_0), the less chance of undesirable photochemistry taking place.[12] Slower energy dissipation allows potential to induce a higher chance for detrimental photochemistry to occur, such as facilitating DNA damage.[11] In the adult *Arabidopsis* plant, sinapoyl malate is concentrated in the leaf epidermis and used as a sunscreening agent in response to overexposure to UV radiation.[13] It strongly absorbs UV photons and efficiently dissipates the energy into heat via trans−cis isomerization.[14,15] Furthermore, the deprotonation of its *para*-hydroxy group leads to a largely bathochromic shift to the near-visible spectral region, significantly reducing its UV-absorbing efficiency.[15] However, this concern is eliminated in commercial sunscreen ingredient octyl methoxycinnamate (OMC) whose para-substituent is a methoxy group. The energy dissipation of OMC is also through the nonradiative trans−cis photoisomerization.[6,16,17] Trans−cis photoisomerization is also determined in many naturally occurring cinnamates in solution, including ferulic acid and the photoactive yellow protein chromophore *para*-coumaric acid.[7,18−23] In most studies, the *para*-substitution is either a hydroxy group or a methoxy group. It has been determined that the *para*-substitution has a much larger effect than *meta*- and *ortho*-substitutions on the excited-state dynamics.[24] Inspired by these, an interesting question is will the photodynamics be different if the *para*-hydroxy group of sinapoyl malate is substituted by a methoxy group or even without a substitution group?

Methyl sinapate (MS) is the simplest sinapate ester and composed of a phenyl ring and an acrylate, as shown in Figure 1. Upon photoexcitation to a bright $\pi\pi^*$ state, excited-state trans-MS molecules evolve along the alkene double bond twisting coordinate (α in Figure 1) to a conical intersection (CI) where internal conversion (IC) to the ground state (S_0) occurs, and then the forming hot S_0 molecules can either go back to trans-form or forward to cis-product, akin to sinapoyl malate.[15,25,26] In this work, in order to further explore the *para*-substitution effect on the excited-state dynamics of sinapates, we have synthesized MS, *p*-OMeMS, and *p*-HMS, as shown in Figure 1. In particular for *p*-HMS, no *para*-substitution results in an interaction between V($\pi\pi^*$) and a relative dark V′($\pi\pi^*$)

Received: July 25, 2019
Accepted: August 22, 2019
Published: August 22, 2019

DOI: 10.1021/acs.jpclett.9b02175
J. Phys. Chem. Lett. 2019, 10, 5244−5249

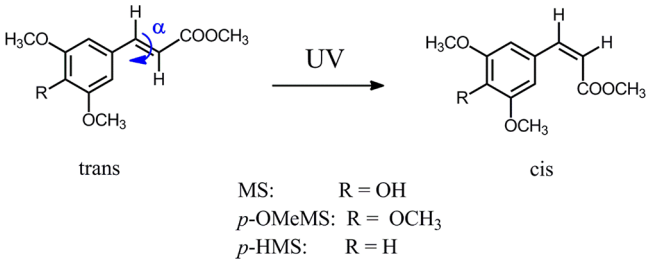

Figure 1. Chemical structures of studied methyl sinapate (MS), *p*-OMeMS, and *p*-HMS.

state, leading to different photodynamics behaviors in the excited state. In addition, although the trans−cis photoisomerization of cinnamates and sinapates is well determined to proceed along an initially populated $\pi\pi^*$ excited-state potential energy surface (PES) in solution,[7,15,27] there exists another energetically closed $\pi\pi^*$ state in the Franck−Condon (FC) region. In the present work, it is the first time to definitely distinguish the dynamics between V($\pi\pi^*$) and V′($\pi\pi^*$) states which is ambiguous in the study of sinapates and cinnamates.[14,19,28,29]

Synthesis and characterization of MS, *p*-OMeMS, and *p*-HMS are detailed in the Supporting Information. Each sample was dissolved in methanol, and the concentration was modulated to reach the absorption maximum at 0.5−0.8 in a quartz cell with a 1 mm optical path. Transient absorption spectra (TAS) were measured by femtosecond pump−probe transient absorption spectroscopy. This setup was described in our previous studies.[26,30] Briefly, the pump pulses for MS, *p*-OMeMS, and *p*-HMS were 320, 320, and 285 nm, respectively. The probe pulse (360−750 nm) was generated by focusing a weak 800 nm pulse on a 2 mm thick CaF_2 crystal. The longest time window is 8 ns. The excited-state lifetimes were determined by a global fitting using the Glotaran software.[31] The time-correlated single photon counting (TCSPC) technique was used to measure nanosecond-time scale fluorescence decays. Time-dependent density functional theory (TDDFT) with the M062X functional[32,33] was employed to explore the electronic properties. The linear-response polarization continuum model (LR-PCM) was used to simulate the solvent response in excited states.[34,35] All the calculations were performed on the Gaussian09 program with the default parameters.[36] More details can be found in the Supporting Information.

The steady-state absorption spectra of MS, *p*-OMeMS, and *p*-HMS exhibit two obvious differences, as shown in Figure 2. One is the gradually blue-shifting absorption peaks of MS, *p*-OMeMS, and *p*-HMS from 328 to 285 nm. The other is the red tail only observed in *p*-HMS. In order to explain their spectral difference, we resort to TDDFT calculations. The LR-PCM/TD-M062X/6-31+g (d, p) method calculates the vertical excitation energies (VEEs) of the two lowest excited states, as shown in Table 1. The excitation energy of the third excited state is much higher and thus not considered. In accordance with previous studies,[28,29] the excited state corresponding to the HOMO to LUMO transition is denoted as the V($\pi\pi^*$) state, which possesses a large oscillator strength and accounts for the first absorption peak. The other excited state with a small oscillator strength is denoted as V′($\pi\pi^*$) state corresponding to the HOMO−1 to LUMO transition. Inspection of Table 1 shows that the V($\pi\pi^*$) state energy

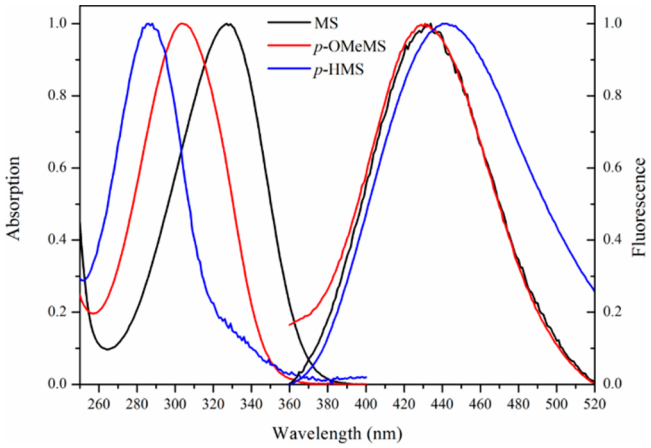

Figure 2. Normalized steady-state UV−visible absorption and emission spectra of MS, *p*-OMeMS, and *p*-HMS.

Table 1. Calculated Vertical Excitation Energies ($\Delta E(f)$ in unit eV; f is the Oscillator Strength) of the Two Lowest Excited States at the LR-PCM/TD-M062X/6-31+g (d, p) Level[a]

$\Delta E(f)$	MS	*p*-OMeMS	*p*-HMS
S1	4.09(0.72); H→L	4.27(0.71); H→L	4.30(0.08); H-1→L
S2	4.55(0.03); H-1→L	4.42(0.10); H-1→L	4.43(0.67); H→L

[a]The transition orbitals are also shown where H represents the HOMO and L represents the LUMO.

sequence is MS < *p*-OMeMS < *p*-HMS, in good agreement with the experimental absorption spectra. After checking their HOMO and LUMO energies (Table S1), it can be concluded that the increased transition energy is mainly induced by a stabilization of the HOMO. In the HOMO of *p*-HMS, a big π-bonding orbital is formed connecting the C_3, C_4, C_5 and *para*-hydrogen atoms (Figure S1). However, when the *para*-hydrogen atom is substituted by a methoxy group (i.e., *p*-OMeMS), an antibonding orbital is formed between C_4 and the *para*-methoxy group, lowering the stability of the HOMO. This destabilization is further improved in the case of the *para*-hydroxy group. In contrast, the V′($\pi\pi^*$) state energy shows a contrasting sequence: MS > *p*-OMeMS > *p*-HMS, finally resulting in a reversal of the ordering of the V($\pi\pi^*$) and V′($\pi\pi^*$) states in *p*-HMS, explaining the red tail only present in the absorption spectrum of *p*-HMS.

As discussed above, in *p*-HMS, the V′($\pi\pi^*$) state lies lower than the V($\pi\pi^*$) state, which likely will result in the participation of the V′($\pi\pi^*$) state in the relaxation dynamics of the V($\pi\pi^*$) state. As shown in Figure 2, the emission spectra of MS and *p*-OMeMS are nearly overlapped while that of *p*-HMS is slightly red-shifted. A significant difference appears after measuring their fluorescence quantum yields (Φ_F), which are determined to be 5.0×10^{-3}, 9.0×10^{-3}, and 0.046 for MS, *p*-OMeMS, and *p*-HMS, respectively. The much larger Φ_F of *p*-HMS indicates a possibly different excited-state dynamics from MS and *p*-OMeMS.

In order to further explore the effect of *para*-substitution on excited-state dynamics, TAS of MS, *p*-OMeMS, and *p*-HMS were measured by femtosecond transient absorption spectroscopy, as shown in Figure 3. The TAS data were fitted globally by a four-exponential function using a sequential model (i.e., $A \xrightarrow{\tau_1} B \xrightarrow{\tau_2} C \xrightarrow{\tau_3} D \xrightarrow{\tau_4}$). As shown in Table 2, the longest

DOI: 10.1021/acs.jpclett.9b02175
J. Phys. Chem. Lett. 2019, 10, 5244−5249

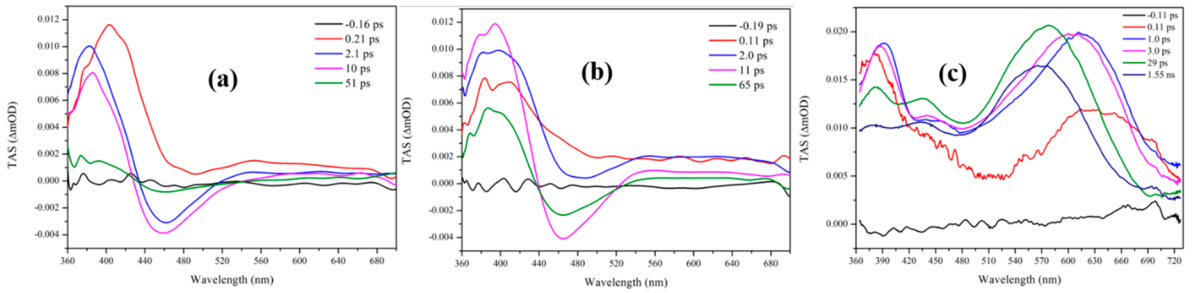

Figure 3. Femtosecond wavelength evolution curves at different time delays of (a) MS, (b) *p*-OMeMS, and (c) *p*-HMS.

Table 2. Fitted Excited-State Lifetimes of the TAS of MS, *p*-OMeMS, and *p*-HMS

	τ_1/ps	τ_2/ps	τ_3/ps	τ_4/ps
MS	0.49	4.82	25.2	>300
p-OMeMS	1.74	8.04	55.8	>300
p-HMS	0.044	3.3	18.0	5000.0

lifetime τ_4 is not accurate due to the inadequate measured time window (300 ps for MS and *p*-OMeMS, 8 ns for *p*-HMS). This model describes the system in a concise parametric manner and obtains evolution-associated spectra (EAS). Although EAS do not necessarily represent the real spectra of each species that occur in the experiment, it is still more physical than decay associated spectra obtained from an unwieldy parallel model where TAS are fitted to be a sum of exponential decays.[21,37]

For MS, upon photoexcitation to the high vibrational levels of the V($\pi\pi^*$) state, an excited-state absorption (ESA) at the 400−440 nm range appears in the early delay Δt = 0.11 ps (Figure 3a). A negative absorption band at the 480−520 nm range also appeared but was not obvious. Then, at Δt = 2.1 ps, the ESA band is blue-shifted to 360−400 nm accompanied by a decreased intensity. The negative absorption band is also blue-shifted to 440−480 nm, but its intensity is largely strengthened. On the basis of steady-state emission spectrum (Figure 2), the negative absorption band can be reasonably assigned as stimulated emission (SE). These spectral shifts and intensity changes from hundreds of femtoseconds to several picoseconds can be attributed to various nonexponential processes taking place at this time scale, including solvation dynamics, intramolecular vibrational redistribution (IVR), and vibrational cooling.[38−40] In addition, the fast intramolecular vibrations of MS may also occur in the time scale, such as the femtosecond in-plane deformation observed in *trans*-coumaric acid.[41] Thus, it is difficult and meaningless to distinguish them as a unique time constant. Therefore, we assign the first two lifetimes (τ_1 = 0.49 ps, τ_2 = 4.82 ps) as a comprehensive result of these processes. Stavros et al. suggest that the lifetime τ_2 may be assigned as a V($\pi\pi^*$)/V′($\pi\pi^*$) IC.[14] However, from our TDDFT calculation results, the V′($\pi\pi^*$) state lies higher than the V($\pi\pi^*$) state in the FC region and the former also has a lower adiabatic energy. As a result, the V($\pi\pi^*$)/V′($\pi\pi^*$) IC can be excluded. At Δt = 51 ps, the TAS is still dominated by the ESA and SE band observed in 10 ps but with much lower intensity. This is induced by the excited-state relaxation along the C═C bond twisting coordinate and characterized by a lifetime τ_3 = 25.2 ps, in quantitative agreement with the results of Stavros et al.[14] As for the component with the longest lifetime τ_4 > 300 ps, its EAS is structureless and has a wide absorption band from 500 to 700 nm and a weak absorption band at <450 nm (Figure S2), which has been observed in methyl coumaric acid.[21] This is a characteristic absorption by radicals generated via two-photon ionization.[19]

The TAS of *p*-OMeMS (Figure 3b) is very similar to that of MS, which is dominated by an ESA band and a SE band. The excited-state relaxation is obviously slower than MS. As shown in Table 2, the τ_1 and τ_2 lifetimes of *p*-OMeMS are longer than those of MS. This is possibly due to the presence of a hydroxy group in MS, which can form hydrogen bonds with methanol and then accelerate the vibrational cooling.[40,42] The excited-state relaxation along the V($\pi\pi^*$) PES to the V($\pi\pi^*$)/S_0 CI is also characterized by τ_3 = 55.8 ps, approximately twice longer than MS. As in the case of MS, the longest lifetime τ_4 is also induced by the absorption of radicals. In addition, the trans−cis photoisomerization is determined by a long-time continuous UV irradiation and ^{1}H NMR spectra (Figures S3, S4). As a result, we propose the same excited-state relaxation mechanism of MS and *p*-OMeMS, as shown in Figure 4a. After

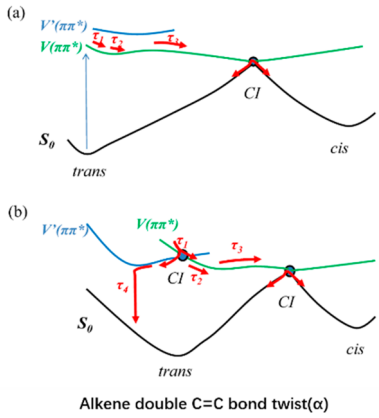

Figure 4. Schematic sketch of the suggested pathways upon excitation to the V($\pi\pi^*$) state of (a) MS and *p*-OMeMS; (b) *p*-HMS.

photoexcitation to the V($\pi\pi^*$) state, solvation dynamics, IVR, vibrational cooling, and fast intramolecular vibrations occur for less than several picoseconds, which are described by τ_1 and τ_2. Then, along the double bond twisting reaction coordinate, the V($\pi\pi^*$) evolves to the V($\pi\pi^*$)/S_0 CI. Note that, in this proposed mechanism, the participation of the V′($\pi\pi^*$) state is completely excluded.

The TAS of *p*-HMS is sharply different from that of MS and *p*-OMeMS, as shown in Figure 3c. At a very early delay (Δt = 0.11 ps), there are a blue ESA band peak at ∼375 nm and a red ESA band peak at ∼630 nm. This is induced by the absorption of the initially populated V($\pi\pi^*$) state. Then both ESA bands are blue-shifted. At the same time, a new band appeared on the blue side. From Δt = 1.0 to 29 ps, the band peak at ∼370 nm is

DOI: 10.1021/acs.jpclett.9b02175
J. Phys. Chem. Lett. 2019, 10, 5244−5249

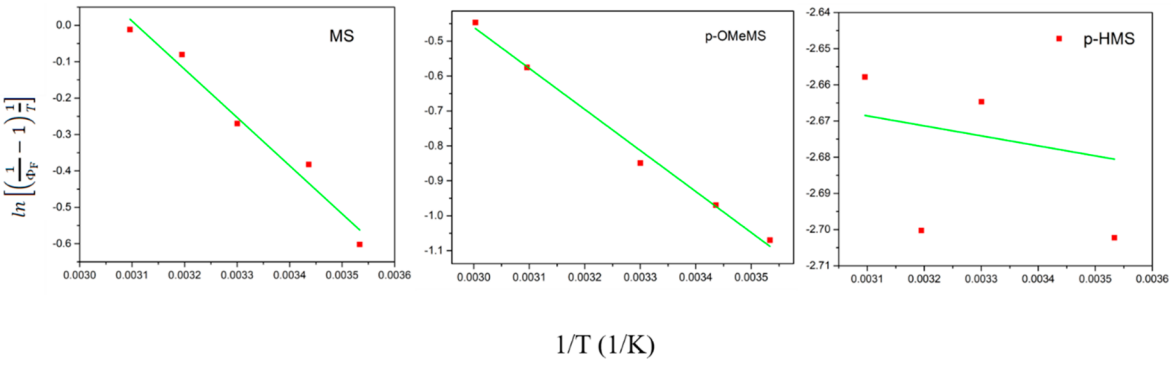

Figure 5. Dependence of the logarithm of fluorescence quantum yield ($\ln((1/\Phi_F - 1)/T)$) on the reciprocal of temperature ($1/T$) of (a) MS; (b) *p*-OMeMS; (c) *p*-HMS. Experimental values are shown in red dots, and the linear fitting results are shown as green lines.

weakened while the band peak at ∼430 nm is strengthened, clearly indicating the formation of a new excited-state species. With the TDDFT results of *p*-HMS considered, the V′($\pi\pi^*$) state lies lower than the V($\pi\pi^*$) state in the FC region. Thus, the V($\pi\pi^*$)/V′($\pi\pi^*$) IC is highly possible. Therefore, we attribute the new species to the V′($\pi\pi^*$) state. This IC occurs for less than 1 ps because the ESA band peak at ∼ 430 nm appeared at Δt = 1.0 ps (Figure 3c). No SE is observed in the TAS of *p*-HMS, possibly due to the much larger positive ESA. At the end of the 8 ns time window, the ESA does not decay to the baseline. Therefore, we used TCSPC to measure the emission decay, as shown in Figure S6. The excitation wavelength is 295 nm, and the emission is recorded at 440 nm. The longest lifetime is fitted to be 5.0 ns. Thus, the lifetime τ_4 is fixed to this value when fitting the TAS of *p*-HMS. After taking into consideration the lifetime of the V($\pi\pi^*$) state of MS and *p*-OMeMS, we attribute the nanosecond-time scale lifetime of *p*-HMS to the V′($\pi\pi^*$) state. The 5 ns lifetime indicates that the V′($\pi\pi^*$) state decays to the S_0 state mainly by emitting a photon. A continuous UV irradiation experiment also detected the formation of *cis*-*p*-HMS (Figure S5). As a result, we tentatively propose a relaxation mechanism of *p*-HMS different from MS and *p*-OMeMS, as shown in Figure 4b. After photoexcitation to the V($\pi\pi^*$) state, it evolves to a V($\pi\pi^*$)/V′($\pi\pi^*$) CI where a branching occurs. A fraction of molecules evolves to the V′($\pi\pi^*$) state via the IC, whereas the remainder proceeds along the V($\pi\pi^*$) PES. The V′($\pi\pi^*$) state is supposed to relax to the S_0 state by fluorescence emission, based on the large Φ_F and 5 ns excited-state lifetime. This is consistent with the bathochromic shift of p-HMS fluorescence because the fluorescence emission stems from the lower V′($\pi\pi^*$) state which is formed from the V($\pi\pi^*$) state. The V($\pi\pi^*$) state evolves to the V($\pi\pi^*$)/S_0 CI along the trans−cis photoisomerization coordinate, just as in the case of MS and *p*-OMeMS. As a result, the sequential model is no longer suitable to fit the TAS data, and a target analysis is employed.[37,43] By fixing the decay lifetime of the V′($\pi\pi^*$) state to be 5.0 ns, three short lifetimes (τ_1−τ_3) are obtained and shown in Table 2. According to the model, τ_1 characterizes the V($\pi\pi^*$)/V′($\pi\pi^*$) IC process. Then, solvation dynamics and vibrational relaxation drive the V($\pi\pi^*$) state to a relaxed V($\pi\pi^*$) state, which is characterized by the lifetime τ_2 = 3.3 ps. Afterward, the V($\pi\pi^*$) state evolves to the CI along the photoisomerization coordinate, which is characterized by τ_3 = 18.0 ps. The para hydrogen substitution on the model plant sunscreens result in the participating of a long-lived V′($\pi\pi^*$) state (5 ns) in the dynamics of excited-state relaxation. The significant reduction in the efficiency of energy dissipation is unsatisfactory for the design of ideal sunscreens.[9,10]

On the basis of the proposed relaxation mechanism, nonradiative relaxation needs to surmount an energy barrier (ΔG) to reach the V($\pi\pi^*$)/S_0 CI, which is in competition with fluorescence emission. According to the transition-state theory and Eyring−Polanyi equation, $\ln((1/\Phi_F - 1)/T)$ should have a linear dependence on the reciprocal of temperature ($1/T$) and the slope is $\Delta G/R$ where R is the gas constant. The detailed deduction can be found in the Supporting Information. Consequently, we measured the Φ_F at different temperatures from 273 to 323 K and then draw the relationship between $\ln((1/\Phi_F - 1)/T)$ and $1/T$, as shown in Figure 5. For MS and *p*-OMeMS, the $\ln((1/\Phi_F - 1)/T)$ exhibits a good linear relationship with $1/T$, corroborating the proposed relaxation model. The energy barrier ΔG is fitted to be 2.64 kcal/mol for MS[25] and 2.34 kcal/mol for *p*-OMeMS. Given the significantly longer excite-state lifetime of *p*-OMeMS than MS, the smaller energy barrier indicates that the dynamics along the V($\pi\pi^*$) state of p-OMeMS is not controlled by the static character of the PES. This dynamically controlled photoisomerization has also been suggested for *para*-methoxy methylcinnamate.[7] In contrast, the linearity between $\ln((1/\Phi_F - 1)/T)$ and $1/T$ of *p*-HMS is very poor, as shown in Figure 5c. This result is reasonable due to the fluorescence emission being mainly from the V′($\pi\pi^*$) state while nonradiative relaxation is along the V($\pi\pi^*$) state; thus, the transition state theory is no longer applicable.

In conclusion, we have investigated the excited-state dynamics of MS, *p*-OMeMS, and *p*-HMS by femtosecond transient absorption spectroscopy and TDDFT calculations. The formation of cis isomers was confirmed by the ^{1}H NMR spectra. Substitution dependent photodynamics in the excited state is demonstrated. For MS and *p*-OMeMS, the initially populated bright V($\pi\pi^*$) state lies lower than the dark V′($\pi\pi^*$) state. Along the trans−cis photoisomerization coordinate, the V($\pi\pi^*$) state efficiently decays to the V($\pi\pi^*$)/S_0 CI where nonradiative transition occurs, leading to a low fluorescence quantum yield. The role of the V′($\pi\pi^*$) state is excluded in MS and *p*-OMeMS. However, for *p*-HMS, the V′($\pi\pi^*$) state is formed after the V($\pi\pi^*$) state passes a V($\pi\pi^*$)/V′($\pi\pi^*$) CI in less than 1 ps. The V($\pi\pi^*$) state of *p*-HMS undergoes a similar nonradiative trans−cis photoisomerization as in MS and *p*-OMeMS. In contrast, fluorescence emission is the main relaxation pathway of the V′($\pi\pi^*$) state, whose excited-state lifetime is as long as 5.0 ns. These results indicate that an in-depth study on excited-state

DOI: 10.1021/acs.jpclett.9b02175
J. Phys. Chem. Lett. 2019, 10, 5244−5249

decay mechanisms of sunscreens is necessary even though the molecules possess similar structures. To the best of our knowledge, it is the first time the dynamics between the V($\pi\pi^*$) and V′($\pi\pi^*$) states have been distinguished, which is ambiguous in the study of sinapates and cinnamates. These results suggest that in order to dissipate the UV energy efficiently, the participation of the V′($\pi\pi^*$) state should be avoided.

■ ASSOCIATED CONTENT

Supporting Information

The Supporting Information is available free of charge on the ACS Publications website at DOI: 10.1021/acs.jpclett.9b02175.

Synthesis and characterization of MS, *p*-OMeMS and *p*-HMS, experimental and TDDFT calculation details, EAS of MS and *p*-OMeMS, target analysis of TAS data of *p*-HMS (PDF)

■ AUTHOR INFORMATION

Corresponding Author

*E-mail: klhan@dicp.ac.cn.

ORCID

Jian Luo: 0000-0002-3928-793X

Donghui Wei: 0000-0003-2820-282X

Keli Han: 0000-0001-9239-1827

Author Contributions

⊥X.Z. and J.L. contributed equally to this work.

Notes

The authors declare no competing financial interest.

■ ACKNOWLEDGMENTS

The work is supported by the National Natural Science Foundation of China (Nos. 21833009, 21533010, 21703244, and 21403226), the National Key Research and Development Program of China (Grant Nos. 2016YFE0120900 and 2017YFA0204800), DICP DMTO201601, DICP ZZBS201703, and the Science Challenging Program (JCKY2016212A501).

■ REFERENCES

(1) Ren, J.; Dai, W.; Xuan, Z.; Yao, Y.; Korpelainen, H.; Li, C. The Effect of Drought and Enhanced UV-B Radiation on the Growth and Physiological Traits of Two Contrasting Poplar Species. *For. Ecol. Manage.* **2007**, *239*, 112−119.

(2) Demkura, P. V.; Ballare, C. L. UVR8Mediates UV-B-Induced Arabidopsis Defense Responses against Botrytis Cinerea by Controlling Sinapate Accumulation. *Mol. Plant* **2012**, *5*, 642−652.

(3) Dahle, J.; Kvam, E. Induction of Delayed Mutations and Chromosomal Instability in Fibroblasts after UVA-, UVB-, and X-radiation. *Cancer Res.* **2003**, *63*, 1464−1469.

(4) Lautenschlager, S.; Wulf, H. C.; Pittelkow, M. R. Photoprotection. *Lancet* **2007**, *370*, 528−537.

(5) Baker, L. A.; Horbury, M. D.; Greenough, S. E.; Coulter, P. M.; Karsili, T. N. V.; Roberts, G. M.; Orr-Ewing, A. J.; Ashfold, M. N. R.; Stavros, V. G. Probing the Ultrafast Energy Dissipation Mechanism of the Sunscreen Oxybenzone after UVA Irradiation. *J. Phys. Chem. Lett.* **2015**, *6*, 1363−1368.

(6) Tan, E. M. M.; Hilbers, M.; Buma, W. J. Excited-State Dynamics of Isolated and Microsolvated Cinnamate-Based UV-B Sunscreens. *J. Phys. Chem. Lett.* **2014**, *5*, 2464−2468.

(7) Miyazaki, Y.; Inokuchi, Y.; Akai, N.; Ebata, T. Direct Spectroscopic Evidence of Photoisomerization in para-Methoxy Methylcinnamate Revealed by Low-Temperature Matrix-Isolation FTIR Spectroscopy. *J. Phys. Chem. Lett.* **2015**, *6*, 1134−1139.

(8) Chang, X.-P.; Li, C.-X.; Xie, B.-B.; Cui, G. Photoprotection Mechanism of p-Methoxy Methylcinnamate: A CASPT2 Study. *J. Phys. Chem. A* **2015**, *119*, 11488−11497.

(9) Rodrigues, N. D. N.; Staniforth, M.; Stavros, V. G. Photophysics of Sunscreen Molecules in the Gas Phase: a Stepwise Approach Towards Understanding and Developing Next-generation Sunscreens. *Proc. R. Soc. London, Ser. A* **2016**, *472*, 20160677.

(10) Baker, L. A.; Marchetti, B.; Karsili, T. N. V.; Stavros, V. G.; Ashfold, M. N. R. Photoprotection: Extending Lessons Learned from Studying Natural Sunscreens to the Design of Artificial Sunscreen Constituents. *Chem. Soc. Rev.* **2017**, *46*, 3770−3791.

(11) Forestier, S. Rationale for Sunscreen Development. *J. Am. Acad. Dermatol.* **2008**, *58*, S133−S138.

(12) Harris, D. C.; Bertolucci, M. D. *Symmetry and Spectroscopy: an Introduction to Vibrational and Electronic Spectroscopy*; Oxford University Press: New York, NY, 1989.

(13) Fraser, C. M.; Chapple, C. The Phenylpropanoid Pathway in Arabidopsis. *Arabidopsis Book* **2011**, *9*, No. e0152.

(14) Baker, L. A.; Horbury, M. D.; Greenough, S. E.; Allais, F.; Walsh, P. S.; Habershon, S.; Stavros, V. G. Ultrafast Photoprotecting Sunscreens in Natural Plants. *J. Phys. Chem. Lett.* **2016**, *7*, 56−61.

(15) Luo, J.; Liu, Y.; Yang, S.; Flourat, A. L.; Allais, F.; Han, K. Ultrafast Barrierless Photoisomerization and Strong Ultraviolet Absorption of Photoproducts in Plant Sunscreens. *J. Phys. Chem. Lett.* **2017**, *8*, 1025−1030.

(16) Pattanaargson, S.; Limphong, P. Stability of Octyl Methoxycinnamate and Identification of Its Photo-degradation Product. *Int. J. Cosmet. Sci.* **2001**, *23*, 153−60.

(17) Peperstraete, Y.; Staniforth, M.; Baker, L. A.; Rodrigues, N. D. N.; Cole-Filipiak, N. C.; Quan, W. D.; Stavros, V. G. Bottom-up Excited State Dynamics of Two Cinnamate-Based Sunscreen Filter Molecules. *Phys. Chem. Chem. Phys.* **2016**, *18*, 28140−28149.

(18) Garcia-Prieto, F. F.; Munoz-Losa, A.; Luz Sanchez, M.; Elena Martin, M.; Aguilar, M. A. Solvent Effects on De-excitation Channels in the P-coumaric Acid Methyl Ester Anion, an Analogue of the Photoactive Yellow Protein (PYP) Chromophore. *Phys. Chem. Chem. Phys.* **2016**, *18*, 27476−27485.

(19) Horbury, M. D.; Baker, L. A.; Quan, W.-D.; Greenough, S. E.; Stavros, V. G. Photodynamics of Potent Antioxidants: Ferulic and Caffeic Acids. *Phys. Chem. Chem. Phys.* **2016**, *18*, 17691−17697.

(20) Wang, S. Q.; Schatz, S.; Stuhldreier, M. C.; Bohnke, H.; Wiese, J.; Schroder, C.; Raeker, T.; Hartke, B.; Keppler, J. K.; Schwarz, K.; et al. Ultrafast Dynamics of UV-excited Trans- and Cis-ferulic Acid in Aqueous Solutions. *Phys. Chem. Chem. Phys.* **2017**, *19*, 30683−30694.

(21) Vengris, M.; Larsen, D. S.; van der Horst, M. A.; Larsen, O. F. A.; Hellingwerf, K. J.; van Grondelle, R. Ultrafast Dynamics of Isolated Model Photoactive Yellow Protein Chromophores: "Chemical perturbation theory" in the Laboratory. *J. Phys. Chem. B* **2005**, *109*, 4197−4208.

(22) Pande, K.; H, C. D. M.; Groenhof, G.; Aquila, A.; Robinson, J. S.; Tenboer, J.; Basu, S.; Boutet, S.; DePonte, D. P.; Liang, M.; et al. Femtosecond Structural Dynamics Drives the Trans/Cis Isomerization in Photoactive Yellow Protein. *Science* **2016**, *352*, 725−729.

(23) Kuramochi, H.; Takeuchi, S.; Yonezawa, K.; Kamikubo, H.; Kataoka, M.; Tahara, T. Probing the Early Stages of Photoreception in Photoactive Yellow Protein with Ultrafast Time-Domain Raman Spectroscopy. *Nat. Chem.* **2017**, *9*, 660−666.

(24) Miyazaki, Y.; Yamamoto, K.; Aoki, J.; Ikeda, T.; Inokuchi, Y.; Ehara, M.; Ebata, T. Experimental and Theoretical Study on the Excited-state Dynamics of Ortho-,Meta-, and Para-Methoxy Methylcinnamate. *J. Chem. Phys.* **2014**, *141*, 244313.

(25) Zhao, X.; Luo, J.; Yang, S.; Han, K. New Insight into the Photoprotection Mechanism of Plant Sunscreens: Adiabatic Relaxation Competing with Nonadiabatic Relaxation in the cis → trans Photoisomerization of Methyl Sinapate. *J. Phys. Chem. Lett.* **2019**, *10* (15), 4197−4202.

DOI: 10.1021/acs.jpclett.9b02175
J. Phys. Chem. Lett. 2019, 10, 5244−5249

(26) Liu, Y.; Yang, S. Excited-State Deactivation of 5-Vinyluracil: Effects of pi-pi Conjugation and Intramolecular Hydrogen Bond C-H···O = C. *J. Photochem. Photobiol., A* **2016**, *330*, 1−7.
(27) Tan, E. M. M. y.; Amirjalayer, S.; Bakker, B. H.; Buma, W. J. Excited State Dynamics of Photoactive Yellow Protein Chromophores Elucidated by High-resolution Spectroscopy and Ab initio Calculations. *Faraday Discuss.* **2013**, *163*, 321−340.
(28) de Groot, M.; Gromov, E. V.; Koeppel, H.; Buma, W. J. High-resolution Spectroscopy of Methyl 4-hydroxycinnamate and Its Hydrogen-bonded Water Complex. *J. Phys. Chem. B* **2008**, *112*, 4427−4434.
(29) Dean, J. C.; Kusaka, R.; Walsh, P. S.; Allais, F.; Zwier, T. S. Plant Sunscreens in the UV-B: Ultraviolet Spectroscopy of Jet-Cooled Sinapoyl Malate, Sinapic Acid, and Sinapate Ester Derivatives. *J. Am. Chem. Soc.* **2014**, *136*, 14780−14795.
(30) Liu, Y.; Zhao, X.; Luo, J.; Yang, S. Excited-state Dynamics of Sinapate Esters in Aqueous Solution and Polyvinyl Alcohol Film. *J. Lumin.* **2019**, *206*, 469−473.
(31) Snellenburg, J. J.; Laptenok, S. P.; Seger, R.; Mullen, K. M.; van Stokkum, I. H. M. Glotaran: A Java-Based Graphical User Interface for the R Package TIMP. *J. Stat. Softw.* **2012**, *49*, 1−22.
(32) Jacquemin, D.; Perpete, E. A.; Ciofini, I.; Adamo, C.; Valero, R.; Zhao, Y.; Truhlar, D. G. On the Performances of the M06 Family of Density Functionals for Electronic Excitation Energies. *J. Chem. Theory Comput.* **2010**, *6*, 2071−2085.
(33) Liu, Y.; Luo, J. Performance of Time-Dependent Density Functional Theory on Twisted Intramolecular Charge Transfer State of Emerging Visible Light Photoswitches. *J. Photochem. Photobiol., A* **2019**, *371*, 336−340.
(34) Cossi, M.; Barone, V. Time-dependent Density Functional Theory for Molecules in Liquid Solutions. *J. Chem. Phys.* **2001**, *115*, 4708−4717.
(35) Tomasi, J.; Mennucci, B.; Cammi, R. Quantum Mechanical Continuum Solvation Models. *Chem. Rev.* **2005**, *105*, 2999−3093.
(36) Frisch, M. J.; Trucks, G. W.; Schlegel, H. B.; Scuseria, G. E.; Robb, M. A.; Cheeseman, J. R.; Scalmani, G.; Barone, V.; Mennucci, B.; Petersson, G. A.; Nakatsuji, H. et al. *Gaussian 09*, revision D.01; Gaussian Inc.: Wallingford, CT, 2009.
(37) van Stokkum, I. H. M.; Larsen, D. S.; van Grondelle, R. Global and Target Analysis of Time-Resolved Spectra. *Biochim. Biophys. Acta, Bioenerg.* **2004**, *1657*, 82−104.
(38) Kiba, T.; Sato, S.; Akimoto, S.; Kasajima, T.; Yamazaki, I. Solvent-assisted Intramolecular Vibrational Energy Redistribution of S-1 Perylene in Ketone Solvents. *J. Photochem. Photobiol., A* **2006**, *178*, 201−207.
(39) Pigliucci, A.; Duvanel, G.; Daku, L. M. L.; Vauthey, E. Investigation of the Influence of Solute-solvent Interactions on the Vibrational Energy Relaxation Dynamics of Large Molecules in Liquids. *J. Phys. Chem. A* **2007**, *111*, 6135−6145.
(40) Kumpulainen, T.; Lang, B.; Rosspeintner, A.; Vauthey, E. Ultrafast Elementary Photochemical Processes of Organic Molecules in Liquid Solution. *Chem. Rev.* **2017**, *117*, 10826−10939.
(41) Kuramochi, H.; Takeuchi, S.; Tahara, T. Ultrafast Structural Evolution of Photoactive Yellow Protein Chromophore Revealed by Ultraviolet Resonance Femtosecond Stimulated Raman Spectroscopy. *J. Phys. Chem. Lett.* **2012**, *3*, 2025−2029.
(42) Zhang, Y.; Chen, J.; Kohler, B. Hydrogen Bond Donors Accelerate Vibrational Cooling of Hot Purine Derivatives in Heavy Water. *J. Phys. Chem. A* **2013**, *117*, 6771−6780.
(43) Hippius, C.; van Stokkum, I. H. M.; Zangrando, E.; Williams, R. M.; Wuerthner, F. Excited State Interactions in Calix 4 arene-perylene Bisimide Dye Conjugates: Global and Target Analysis of Supramolecular Building Blocks. *J. Phys. Chem. C* **2007**, *111*, 13988−13996.

DOI: 10.1021/acs.jpclett.9b02175
J. Phys. Chem. Lett. 2019, 10, 5244−5249